Soft Matter

Dynamic Article Links

Cite this: *Soft Matter*, 2012, **8**, 1395

www.rsc.org/softmatter

PAPER

Hedgehog defects in mixtures of a nematic liquid crystal and a non-nematogenic component

Ezequiel R. Soulé[ab] and Alejandro D. Rey*[a]

Received 13th September 2011, Accepted 7th November 2011
DOI: 10.1039/c1sm06741a

A theoretical study of the core structure and composition of a hedgehog defect in a mixture of a nematic liquid crystal and a second non-nematogenic component is presented. Fractionation of the components between the bulk and the defect core is rigorously considered by using solution thermodynamics. Two complementary approaches are used to analyze this problem: a multiscale model based on a Landau–de Gennes free energy functional that is solved numerically, and a macroscopic sharp interface phase-equilibrium model, which considers the defect core as an isotropic phase in equilibrium with a distorted nematic phase and that under certain limiting conditions yields equations that reveal the mechanisms that select defect core structure, geometry, and composition. It is found that the non-nematogenic component segregates preferentially to the defect core, and the defect radius increases as the concentration of the second component and the temperature are increased. As previously predicted for pure liquid crystals, close to saturation conditions the radius increases significantly, and a small range of supersaturation or superheating is observed.

1. Introduction

The study of topological defects has been long recognized as an essential aspect of liquid crystal science, as defects are frequently generated during mesophase formation, material processing, and sometimes they appear as equilibrium structures.[1–20] In many applications, defects have an unfavourable effect and a defect-free material is desired (the best known example of this are liquid crystal display devices), but there are processing and geometric conditions where defects appear as a part of the material structure, like in carbonaceous fibers,[5,6] filled nematics,[7–10] isolated droplets[11–14] or cavities[15,16] with strong anchoring. In most cases, whether they are an essential feature of the material structure or not, defects have a very important impact on the material properties and device performance and it is desirable to control their nucleation, stability and core structure through an understanding of defect physics.

The structure and stability of different types of defects in pure LC have been widely studied in the past.[9,12–24] Effects of temperature, transition rules between different defect structures, and dynamic process of formation and annihilation of defects are well known in two and three dimensions.[10–12,21,23] Nevertheless, the studies of defects in mixtures are very limited. Several studies have focused on the formation of phase-separated morphologies in mixtures of liquid crystals and other components, and how the general textures and the appearance of different defects are affected by composition and temperature,[25–27] but a systematic study of the structure of a defect core for mixtures has not been performed. A particular case where this has a remarkable importance is the case of the stabilization of blue phases by the addition of a guest component.[28–31] It was shown experimentally that the addition of polymers or nanoparticles can increase the range of stability of this phase from a few to dozens of degrees.[28,29] Another important case where solute distribution in a defect is crucial is the case of mitosis of living cells, where it is hypothesized that the poles of the cell are nematic defects and the migration of the chromosomes to the poles is just the segregation of a solute to the defects.[32]

Recently, the stabilization of blue phases by the addition of a non-mesogenic component was analyzed theoretically.[30,31] It was shown that replacing the defect core with the guest component lowers the free energy of the blue phase, thus providing the observed stabilizing effect, but the structure of the defect (radius, order parameter profiles, solute distribution) was not analyzed in these studies, and the full effect of temperature and global composition was not analyzed.

In this work, we use two complementary approaches to study a hedgehog defect in a mixture of a LC and a non-mesogenic component. The first approach is based on a Landau–de Gennes free energy functional, where the free energy density is formulated in terms of homogeneous and gradient contributions and the resulting governing equations for the continuous nematic order and orientation are solved numerically. The second method is a sharp interface macroscopic thermodynamic approach where the nematic bulk and the isotropic defect core

[a]*Department of Chemical Engineering, McGill University, Montreal, Quebec, H3A 2B2, Canada. E-mail: alejandro.rey@mcgill.ca*
[b]*Institute of Materials Science and Technology (INTEMA), University of Mar del Plata and National Research Council (CONICET), J. B. Justo 4302, 7600 Mar del Plata, Argentina*

This journal is © The Royal Society of Chemistry 2012

are treated as different phases in equilibrium. The first continuous core approach allows the spatial profiles of concentration and order parameter across the defect to be resolved in detail, while the second sharp interface method is less detailed but leads to revealing analytical expressions for the core composition and radius in certain limiting cases. These two approaches have been used previously for pure liquid crystals, for example, to analyze the dependence of a disclination radius on temperature,[19] or to analyze the relative stabilities of different defect configuration in radial spherulites.[17,20] In this work the defect radius and spatial distribution of the second component are analyzed for a hedgehog configuration, as a function of temperature and binary mixture composition.

This paper is organized as follows. In Section 2 we present the details of the two approaches used: Section 2.1 describes the Landau–de Gennes continuum model, Section 2.2 describes the macroscopic sharp interface thermodynamic model, and in Section 2.3 we describe the conditions and parameters used in the calculations. Section 3 presents the results and discussion of both complementary approaches. Finally, Section 4 presents the conclusions. In addition, two appendices with the rigorous derivations of the model equations are included; Appendix A gives the evolution equations for order parameter S and composition ϕ for the Landau–de Gennes model in radial coordinates, and Appendix B derives the governing equations for defect radius R and composition ϕ for the sharp interface model.

2. Model

2.1. Multiscale model based on a Landau–de Gennes (LdG) free energy functional

The free energy density of a binary mesogenic–non-mesogenic mixture is given by the sum of homogeneous and gradient contributions. The Flory–Huggins theory is used for the isotropic free energy of the mixture, in combination with Maier–Saupe theory for nematic order.[25–27] This widely used model is simple, but it still captures the essential physics of the system; it is able to represent the different phase transitions and it reproduces the parametric sensitivity at least qualitatively. Taking the pure components in the isotropic state as the reference state the free energy reads:

$$f^{h^*} = \frac{v_{ref} f^h}{R_{gas} T} = \frac{v_{ref} f_{mix}}{R_{gas} T} + \frac{(1-\phi)}{r_{LC}} \frac{f_{NEM}}{R_{gas} T} \quad (1)$$

$$\frac{v_{ref} f_{mix}}{R_{gas} T} = \frac{1-\phi}{r_{LC}} \ln(1-\phi) + \frac{\phi}{r_I} \ln(\phi_{LC}) + \chi\phi(1-\phi) \quad (2)$$

$$\frac{f_{NEM}}{R_{gas} T} = \frac{3}{4} \nu(1-\phi)\mathbf{Q} : \mathbf{Q} - \ln(Z) \quad (3)$$

where ϕ is the volume fraction of the non-mesogenic species (we will refer to this component as "I"), the symmetric and traceless tensor $\mathbf{Q} = S\mathbf{nn} + P(\mathbf{ll} - \mathbf{mm})$ is the quadrupolar order parameter,[10] where S and P are the scalar uniaxial and biaxial parameters, $\mathbf{n}$, $\mathbf{m}$ and $\mathbf{l}$ are the eigenvectors of $\mathbf{Q}$, r_{LC} and r_I are the ratios of molar volume of LC and I components with respect to the reference volume v_{ref}, χ is the mixing interaction parameter, $\nu = 4.54 T_{NI}/T$ is the Maier–Saupe quadrupolar interaction parameter, R_{gas} is the gas constant, T is the temperature and T_{NI} is the isotropic–nematic temperature for the pure LC. The orientational partition function Z was approximated by an eighth-degree polynomial in terms of the invariants of $\mathbf{Q}$ (obtaining a "Landau" polynomial expression) using a least-square fit to obtain the polynomial coefficients.[33] In eqn (1)–(3) the usual characteristic free energy density $R_{gas}T/v_{ref}$ was used to make the equations non-dimensional. The gradient free energy is given by gradients in concentration and order:[25,26]

$$f^g = L_\phi(\nabla\phi)^2 + L_{Q1}\nabla\mathbf{Q}\vdots\nabla\mathbf{Q} + L_{Q2}(\nabla\mathbf{Q})(\nabla\mathbf{Q}) + L_{Q\phi}(\nabla\mathbf{Q})\nabla\phi \quad (4)$$

The gradients can be made non-dimensional by defining a characteristic length $l = (v_{ref}(L_{Q1} + L_{Q2})/R_{gas}T_{NI})^{1/2}$, and eqn (4) becomes

$$\begin{aligned} f^{g^*} &= \frac{v_{ref}}{R_g T} f^g \\ &= \frac{L^*_\phi}{T^*}(\nabla^*\phi)^2 + \frac{L^*_{Q1}}{T^*}\nabla^*\mathbf{Q}\vdots\nabla^*\mathbf{Q} + \frac{L^*_{Q2}}{T^*}(\nabla^*\mathbf{Q})(\nabla^*\mathbf{Q}) \\ &\quad + \frac{L^*_{Q\phi}}{T^*}(\nabla^*\mathbf{Q})\nabla^*\phi \end{aligned} \quad (5)$$

where $L_i^* = L_i/(L_{Q1} + L_{Q2})$ for $i = \phi$, $Q1$, $Q2$ and $Q\phi$, $T^* = T/T_{NI}$, and $\nabla^* = l\nabla$ is the gradient with respect to the non-dimensional spatial coordinates. Note that the characteristic length defined here is related to the elastic constants, while the reference volume defined previously is an arbitrary molar volume (originally arising from the cell volume in a lattice model), and they are not related.

The evolution of $\mathbf{Q}$ and ϕ is given by:[25–27]

$$\begin{aligned} \frac{\partial\mathbf{Q}}{\partial t^*} &= \frac{\partial f^*}{\partial\mathbf{Q}} - \nabla^*\frac{\partial f^*}{\partial\nabla^*\mathbf{Q}} \\ \frac{\partial\phi}{\partial t^*} &= M_r\nabla^{*2}\left(\frac{\partial f^*}{\partial\phi} - \nabla^*\frac{\partial f^*}{\partial\nabla^*\phi}\right) \end{aligned} \quad (6)$$

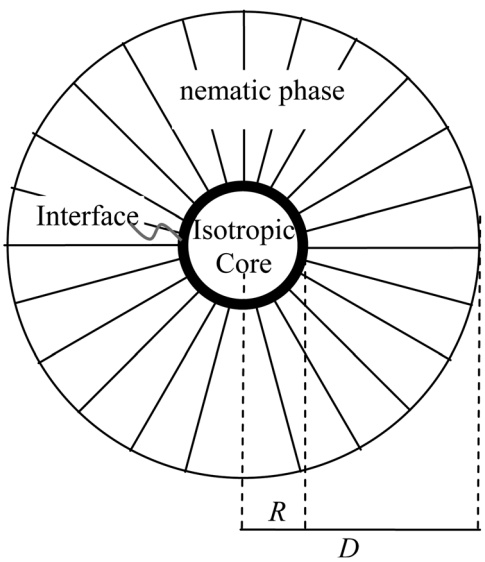

Fig. 1 Schematics of the radial spherulite with a hedgehog defect at the center, and the relevant geometric variables used in the sharp interface thermodynamic approach.

This journal is © The Royal Society of Chemistry 2012

where t^* is the dimensionless time and M_r is a mobility ratio. Although the stationary solution is the objective of this work, the dynamic evolution is calculated, as relaxation techniques can have serious convergence problems if the initial guess is not adequate. Note that the stationary solution is independent of M_r.

As the objective of this work is to analyze a radially symmetric system, eqn (1)–(6) are written in spherical coordinates and only the derivatives with respect to r are kept. In addition it is assumed that P is 0 (uniaxial state). The full equations written in radial coordinates are presented in Appendix A. Symmetric breaking and biaxiality effects are left for future work.

2.2 Macroscopic sharp interface model based on phase equilibrium thermodynamics

In the sharp interface approach, following Mottram and Sluckin,[19] the defect core is considered as fully isotropic, so the whole defect is treated as a region of isotropic phase, as shown in Fig. 1. The full derivation of the model equations is presented in Appendix B, here we present the main concepts and equations. The system is considered as two separated phases, a uniaxial nematic phase with radial orientation and an isotropic phase representing the defect, separated by a well defined interface. This is shown schematically in Fig. 1.

The total free energy of this radial spherulite is:

$$F = \frac{4}{3}\pi R^3 f_i + \frac{4}{3}\pi\left(D^3 - R^3\right) f_n + 4\pi R^2\sigma + 16\pi(L_1 + L_2)S^2(D - R) \quad (7)$$

The first term is the energy of the defect core, the second term is the homogeneous contribution from the nematic region, the third term is the interfacial energy between the core and the nematic phase, and the last term is the gradient energy from the distortions of the director in the nematic phase due to curvature, from integration of eqn (A3) (it is assumed that the value of the scalar order parameter is constant in the nematic phase). As noted by Mottram and Sluckin,[19] the last term favours a large radius, while the first terms (free energy difference and surface tension) favour small defect cores. The mass balance imposes a restriction on the volume and concentrations of the phases:

$$\phi_0 D^3 = \phi_i R^3 + \phi_n(D^3 - R^3) \quad (8)$$

where 0, i, and n correspond to initial, isotropic and nematic phases, respectively. Thus, for a given value of D, only two of the three variables ϕ_n, ϕ_i and R are independent. The equilibrium conditions are given by the minimization of the free energy, given by eqn (7). For a defect in a nematic spherulite, the assumption $D \gg R$ can be made. From eqn (8), this assumption leads to $\phi_n = \phi_0$. This results in the equilibrium conditions for the defect composition and radius (see eqn (9) and (10) in Appendix B for detailed derivations):

$$\frac{\partial f_i^*}{\partial\phi} - \frac{\partial f_n^*}{\partial\phi} + \frac{3}{R^*}\frac{\partial\sigma^*}{\partial\Delta\phi} = 0 \quad (9)$$

$$\left(f_i^* - f_n^*\right) + \frac{\partial f_n^*}{\partial\phi}\left(\phi_n - \phi_i\right) + 2\frac{\sigma^*}{R^*} - 4T^*\frac{S^2}{R^{*2}} = 0 \quad (10)$$

where the dimensionless variables are $f_i^* = v_{ref}f_i/R_{gas}T$, $f_n^* = v_{ref}f_n/R_{gas}T$, $\sigma^* = (1/l)v_{ref}\sigma/R_{gas}T$, and $R^* = R/l$. These equations will in general not have an analytical solution, but nevertheless simplifications can be made for two important limiting cases: (i) near saturation conditions and (ii) small solute concentration, as follows. (i) In the case the mixture is close to bulk saturation conditions (this means close to the boundaries of the region of phase coexistence), the free energy can be expanded as a function of concentration in the vicinity of saturation conditions and (see Appendix B) the following equations are obtained:

$$\phi_i - \phi_{i,sat} = \frac{\partial^2 f_{n,sat}^*/\partial\phi^2}{\partial^2 f_{i,sat}^*/\partial\phi^2}\left(\phi_n - \phi_{n,sat}\right) \quad (11)$$

$$R^* = \frac{\sigma^* \pm \sqrt{\sigma^{*2} - (4/T^*)\left(\partial^2 f_{n,sat}^*/\partial\phi^2\right)\left(\phi_{i,sat} - \phi_{n,sat}\right)\left(\phi_n - \phi_{n,sat}\right)S^2}}{\left(\partial^2 f_{n,sat}^*/\partial\phi^2\right)\left(\phi_{i,sat} - \phi_{n,sat}\right)\left(\phi_n - \phi_{n,sat}\right)} \quad (12)$$

where the subscript "sat" means that the variable is evaluated in bulk saturation conditions. These equations are independent of the particular model used to describe the free energy. If the surface tension σ^* and the order parameter S are approximated by the values at saturation, then ϕ_i and R are given in terms of thermodynamic properties at the saturation conditions, which are functions of temperature only and can be easily calculated or measured experimentally. In order to derive these equations the assumption that the effects of interfacial tension can be neglected in eqn (11) has been made (see Appendix B); the validity of this assumption will be addressed *a posteriori*.

Eqn (12) shows that, even for a supersaturated nematic phase, a finite radius defect can exist, so a supersaturated nematic phase can be metastable. This is analogous to the case of the pure liquid crystal.[19] There are two possible values for the radius R, one of them corresponds to a stable defect, the other corresponds to a maximum in the free energy and is thus unstable.

(ii) In the case of very low concentration of I, eqn (9) and (10) can be simplified, but some expression must be assumed for the mixing free energy in order to obtain an analytical solution. Using Flory–Huggins energy of mixing the result is (Appendix B):

$$\phi_i = \phi_n \exp\left[r_I\left((1 - \phi_n)\frac{\partial f_{NEM}^*}{\partial\phi} - f_{NEM}^*\right)\right] \quad (13)$$

$$R^* = \frac{\sigma^* \pm \sqrt{\sigma^{*2} - (4/T^*)\left[-f_{NEM}^* + \left(1 + r_I\left(\partial f_{NEM}^*/\partial\phi\right) - \exp\left[r_I\left(\left(\partial f_{NEM}^*/\partial\phi\right) - f_{NEM}^*\right)\right]\right)(\phi_n/r_I)\right]S^2}}{-f_{NEM}^* + \left(1 + r_I\left(\partial f_{NEM}^*/\partial\phi\right) - \exp\left[r_I\left(\left(\partial f_{NEM}^*/\partial\phi\right) - f_{NEM}^*\right)\right]\right)(\phi_n/r_I)} \quad (14)$$

In order to calculate all the parameters appearing in eqn (13) and (14) we make the following assumptions. (1) Considering that the interfacial tension is proportional to the integral of the gradient energy, for small concentrations the main contribution will be the integral of $(dS(x)/dx)^2$, which is equivalent to the surface tension of the pure LC. Assuming that the function $S(x)$ does not change very much across the interface, the interface tension is proportional to S^2 evaluated in the nematic phase. Consequently, for $T < 1$ we can write $\sigma(T) = \sigma(T = 1, \phi = 0)(S/S(T = 1, \phi = 0))^2$, and the only value of surface tension that needs to be known is the one corresponding to the pure LC at T_{NI}. (2) Usually the properties of the mixtures can be easily related to the properties of the pure LC at some different temperature, for example, in Maier–Saupe theory, $S(T, \phi) = S(T/(1 - \phi), 0)$, $f_{NEM}(T, \phi) = f_{NEM}(T/(1 - \phi), 0)$ and $(1 - \phi)\partial f_{NEM}/\partial\phi = T\partial f_{NEM}/\partial T$; if this assumption can be made, all the properties appearing in eqn (13)–(14) can be evaluated for the pure liquid crystal (no properties of the mixture are involved). (3) As an alternative, if the free energy and its derivative are difficult or costly to calculate or measure, this function can be linearly expanded as a function of ϕ in the vicinity of 0, and eqn (13) and (14) become

$$\phi_i = C_1\phi_n - C_2{\phi_n}^2 \tag{15}$$

$$R^* = \frac{\sigma^* \pm \sqrt{\sigma^{*2} - (4/T^*)\left[-f^*_{NEM}|_0 + (1 - C_1)(\phi_n/r_I) + \left(r_I\left(\partial^2 f^*_{NEM}/\partial\phi^2\right)\big|_0 + C_2\right)\left(\phi_n^2/r_I\right)\right]S^2}}{-f^*_{NEM}|_0 + (1 - C_1)(\phi_n/r_I) + \left(r_I\left(\partial^2 f^*_{NEM}/\partial\phi^2\right)\big|_0 + C_2\right)\left(\phi_n^2/r_I\right)} \tag{16}$$

where

$$C_1 = \exp\left[r_I\left(\frac{\partial f^*_{NEM}}{\partial\phi}\bigg|_0 - f^*_{NEM}|_0\right)\right];$$

$$C_2 = \left(\frac{\partial^2 f^*_{NEM}}{\partial\phi^2}\bigg|_0 - 2\frac{\partial f^*_{NEM}}{\partial\phi}\bigg|_0\right)\exp\left[r_I\left(\frac{\partial f^*_{NEM}}{\partial\phi}\bigg|_0 - f^*_{NEM}|_0\right)\right]$$

and the subscript "0" means for $\phi = 0$. In this case, the free energy and its derivatives have to be measured or evaluated only at $\phi = 0$, or they could be treated as adjustable parameters. Only linear terms could be retained in eqn (15) and (16), but it was found that this limits significantly the range in which these equations can be applied. Eqn (13)–(14) and (15)–(16) were found to give equivalent results in the conditions analyzed in this work. The full derivation of eqn (11)–(16) given in Appendix B shows how the defect structure can be made more explicit by using the sharp interface model.

2.3. Simulation details

The construction of the phase diagram follows standard procedures: the equilibrium condition at each temperature is given by the equality of chemical potentials of each component and the minimization of the free energy with respect to the order parameter, in each phase.

Simulations with the LdG model were performed in radial coordinates, using a domain comprised between $r^* = 0$ and 2000 (for this value of r^*, the defect structure is independent of domain size). The initial condition was a smooth step function in S at $r^* = 2$, and homogeneous composition. Natural and no-flux boundary conditions were used. The equations were solved with COMSOL Multiphysics, using quadratic Lagrange basis functions; standard numerical techniques were used to ensure convergence and stability.

Surface tensions were calculated from the LdG model, for a planar equilibrium interface, as:

$$\sigma^* = 2\int_{-\infty}^{\infty} f^{g*}dx \tag{17}$$

for different temperatures. These values were used in eqn (11)–(16) as indicated. The following dimensionless parameters were used: $r_{LC} = 2$, $r_I = 1$, $\chi = 0.8/T^*$, $L_\phi{}^* = L_{Q1}{}^* = L_{Q2}{}^* = 0.50$ (with these parameter values, equilibrium isotropic–isotropic phase separation does not take place). If dimensional parameters matching some representative values of existing LC are used, the calculated defect core radius and interface tensions reproduce the experimentally observed values. For example, for $L_i \approx 10^{-11}$ J m^{-1}, $v_{ref} = 100$ cm^3 mol^{-1} (which means that the LC has a specific volume of 200 cm^3 mol^{-1}), $T_{NI} = 300$ (these values are approximately the corresponding values for 5CB) a value of $l \approx 1$ nm is obtained. This leads to defect cores of radius between 2 and 50 nm and interfacial tensions between 5×10^{-5} and 5×10^{-4} J m^{-2}, which are in the order of magnitude of experimental measurements.

3. Results and discussion

Fig. 2 shows the thermodynamic phase diagram used in this study computed using eqn (1)–(3). Two types of phases exist: isotropic ($\mathbf{Q} = 0$) and nematic ($\mathbf{Q} > 0$).

Simulations were performed for different values of ϕ_0 at constant temperatures (horizontal lines at 0.7, 0.775, 0.85 and 0.925) and at constant ϕ_0 (vertical lines at 0.005, 0.01, 0.02 and 0.05) for different temperatures. All these (ϕ_0, T) points lie in the dotted lines shown in the inset in Fig. 2. All the results shown correspond to dimensionless variables.

Fig. 3 shows profiles of concentration and order parameter at $T = 0.925$ for different values of ϕ_0, and Fig. 4 for $\phi_0 = 0.02$ at different temperatures. The radius of the defect increases when the temperature or concentration increases (that is, as the system approaches to saturation conditions), and the concentration of the second component is always higher in the defect core than in the nematic bulk (as this component is non-mesogenic it segregates preferentially to the isotropic phase). This is in accordance

This journal is © The Royal Society of Chemistry 2012

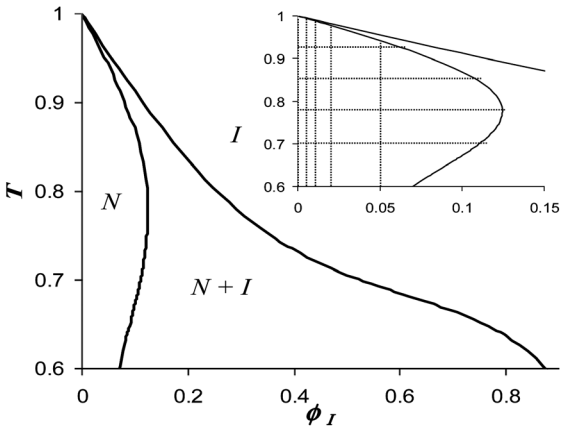

Fig. 2 Phase diagram used in this work, calculated with $\chi = 0.8/T^*$, $r_I = 1$, $r_{LC} = 2$. The temperature axis is normalized with respect to T_{NI} of the pure LC. Regions of existence of the homogeneous isotropic phase (I), homogeneous nematic phase (N), and coexistence ($I + N$) are indicated. The inset shows the small composition range. The simulations were run using (ϕ_0, T) located in the dotted lines in the inset.

with the argument that high-energy defect cores are "replaced" by the guest component, as discussed for stabilized blue phases,[29–31] lowering the free energy of the core (although it is clear that the replacement is not complete). The increase of the radius with concentration, as observed in eqn (6), could be explained considering that the free energy of the core, which favours small radius, is decreased by this preferential segregation; consequently

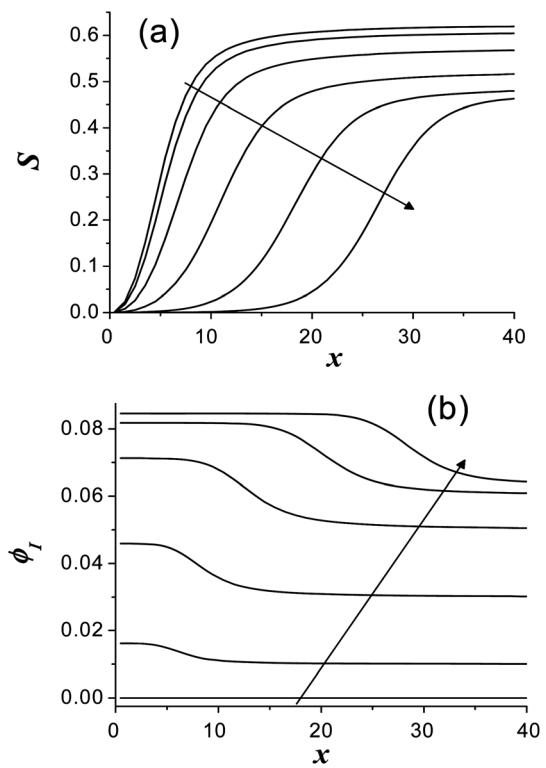

Fig. 3 Profiles of order parameter (a) and concentration (b), for $T/T_{NI} = 0.925$, and the following values of ϕ_0, increasing in the direction of the arrow: 0, 0.01, 0.03, 0.05, 0.06 and 0.063 (note in b that for $\phi_0 = 0$, $\phi_I = 0$).

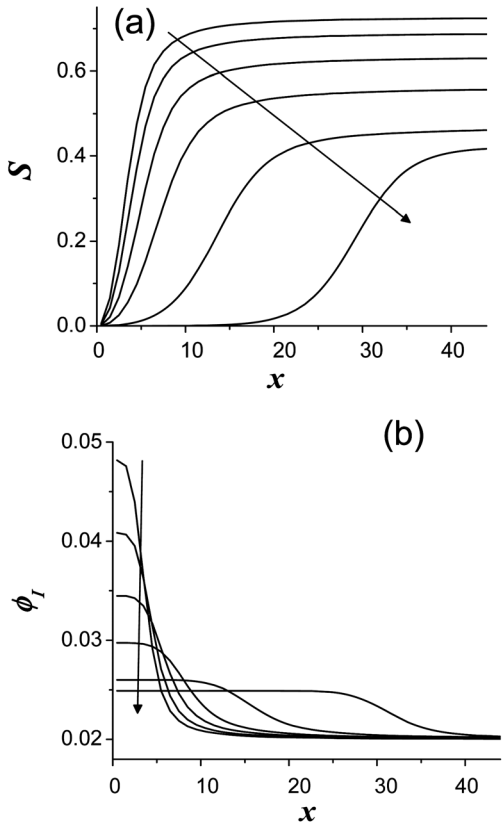

Fig. 4 Profiles of order parameter (a) and concentration (b), for $\phi_0 = 0.02$, and the following values of T^*, increasing in the direction of the arrow: 0.8, 0.85, 0.9, 0.94, 0.97 and 0.9775.

the terms favouring large radius become relatively more important.

Fig. 5 shows the excess free energy of the equilibrium defect (defined as the difference between the total free energy of the radial spherulite, calculated with the LdG model, and the free energy of the same volume of homogeneous nematic phase), as a function of concentration. The defect free energy decreases with concentration in the temperature range explored, in accordance with the previous argument. The stabilization is more noticeable at higher temperatures (lower curve with squares), when the free energy of the defect is lower.

In order to better characterize the effects of concentration and temperature, the defect radius R and concentration ϕ_i at the defect core are plotted as a function of these variables in Fig. 6 and 7, using both the Landau–de Gennes model and the sharp interface model. Fig. 6 shows plots at constant temperatures, as a function of concentration close to the saturation conditions and Fig. 7 shows plots at constant small concentrations as a function of temperature.

Fig. 6a shows the concentration of the isotropic core (expressed as a deviation from the saturation concentration), and Fig. 6b shows the dimensionless radius, as a function of $\phi_0 - \phi_{n,sat}$. The results from simulations and from the analytical theory (eqn (11) and (12)) are presented. The concentration of the isotropic core in the simulations was measured at $r = 0$, and the radius was taken as the position at which the second derivative of $S(x)$ is a minimum.[19] A good agreement between simulations and

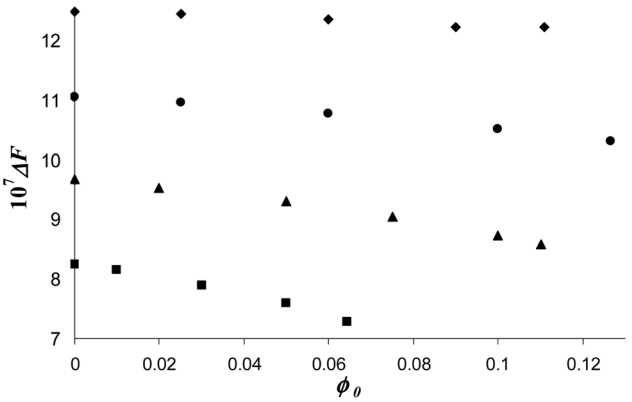

Fig. 5 Excess free energy of the equilibrium defect as a function of concentration. The different temperatures are $T = 0.925$ (squares), 0.85 (triangles), 0.775 (circles), and 0.7 (diamonds).

analytical theory is observed, this agreement gets worse outside the range of compositions analyzed in each plot.

Fig. 6a shows how the concentration in the defect core depends on the concentration of the nematic phase for different

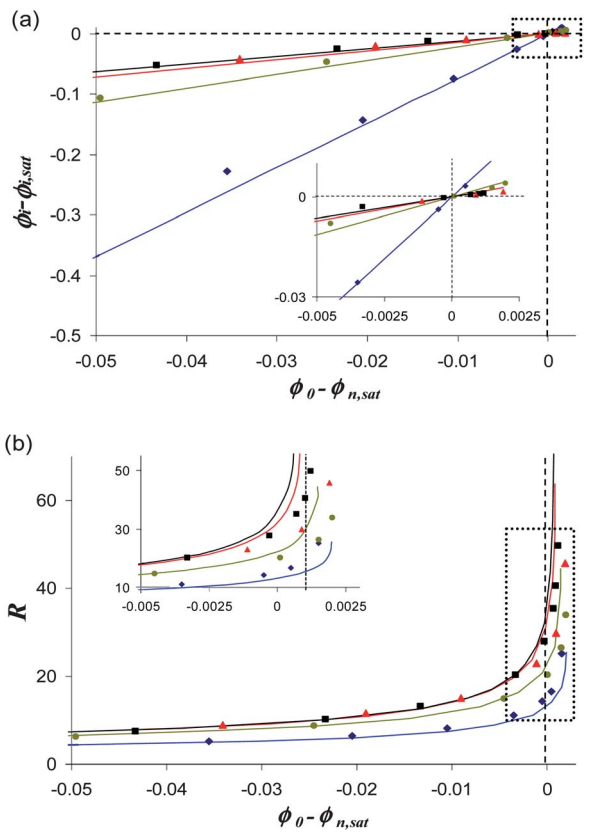

Fig. 6 Deviations of the concentration of the isotropic core with respect to saturation conditions (a), and defect core radius (b), as a function of the deviation of the global concentration from saturation conditions. The dashed lines show saturation compositions. The insets correspond to the areas in the vicinity of saturation, as indicated by the dotted squares. The points are the result from LdG simulations; the full lines are the results from the analytical theory. The lines are plotted up to the limit of maximum stability (beyond this point the model has no solution for finite radius). The different temperatures are $T = 0.925$ (squares), 0.85 (triangles), 0.775 (circles), and 0.7 (diamonds).

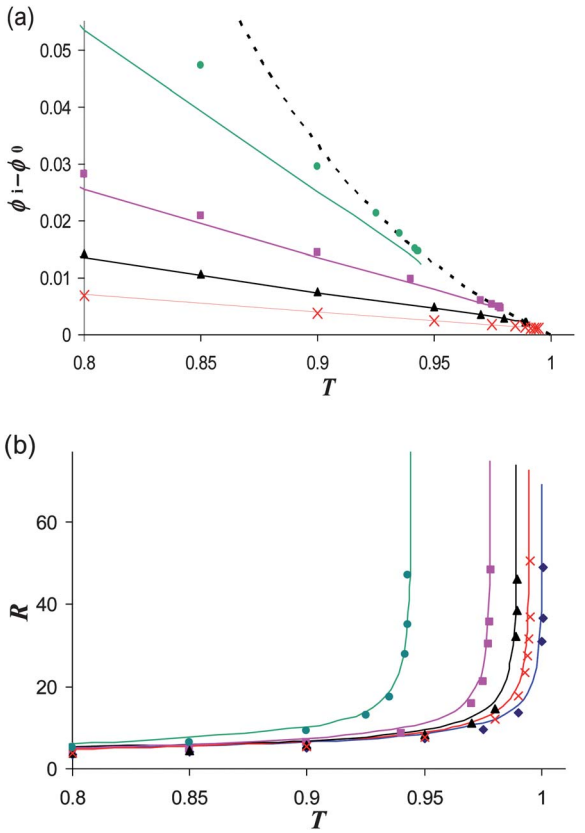

Fig. 7 Concentration jump in the isotropic core, $\phi_i - \phi_0$ (a), and defect core radius (b) as a function of temperature, for different values of ϕ_0. The points are the result from the LdG model, the full lines are the results from the analytical theory. The lines are plotted up to the limit of maximum stability (beyond this point the model has no solution for finite radius). The dotted line in (a) shows the saturation composition. The values of initial concentration are $\phi_0 = 0$ (diamonds), 0.005 (crosses), 0.01 (triangles), 0.02 (squares), and 0.05 (circles).

temperatures. For high temperatures (close to T_{NI}), the slope of the line is close to 1, meaning that the deviation from saturation is similar in both phases. For lower temperatures, the deviation in the isotropic phase is higher than the deviation in the nematic phase (nevertheless, the concentration in the core is always larger as $\phi_{i,sat}$ is larger for lower temperatures). The linear approximation works quite well in the analyzed range. As can be observed in the simulation results, when the nematic phase is saturated, the concentration in the core corresponds very approximately to $\phi_{i,sat}$, which means that the assumption of neglecting interfacial effects in eqn (11) (see Appendix B and Section 2.2) is adequate for real systems (recall that the values used for the physical parameters in this work match approximately with those of experimental systems, see Section 2.3), and solute distribution is driven by bulk thermodynamics.

The defect core radius, as shown in Fig. 6b, increases abruptly in the vicinity of saturation. As shown in the inset, the nematic phase can be supersaturated up to a value that depends on the temperature (note that the value of the radius at the maximum supersaturation is finite). Far from saturation, the dependence of the radius on the concentration is not as dramatic, but still the radius is affected by the presence of the second component.

This journal is © The Royal Society of Chemistry 2012

Fig. 7a shows the increase of the concentration in the core with respect to the nematic phase, for the case of low global concentrations of guest component. The concentration difference increases when the temperature decreases, with a slope that is higher for higher values of ϕ_0. The core radius as a function of temperature is shown in Fig. 7b. The behaviour is similar to that observed in Fig. 6, the radius increases abruptly when approaching the saturation temperature, with the possibility of a small supersaturation. Far from the saturation temperature, increasing ϕ_0 increases slightly the radius.

All these results are in accordance with what Mottram and Sluckin observed in pure liquid crystals.[19] The behaviour of mixtures is similar in that the radius increases abruptly close to equilibrium conditions. The main effect of adding a second, non-nematogenic component is its preferential segregation to the defect (to a degree that depends on temperature and composition), producing a stabilizing effect and an increase in the defect core radius. This shows not only that the defect structure can be affected by the presence of a second component (as in the stabilization effect reported in blue phases), but also that the spatial distribution of a solute can be controlled by controlling the defect distribution.

Conclusions

Theory and simulations of a hedgehog defect in a mixture of a nematic LC and a non-nematogenic component were performed, for different compositions and temperatures. The analytical theory was based on a sharp interface macroscopic thermodynamic approach, considering the defect and the bulk as different thermodynamic phases, and the numerical simulations were based on a continuous Landau–de Gennes free energy functional. These two complementary methods, that have been previously used to analyze defects in pure liquid crystals by Mottram and Sluckin,[19] were adapted for mixtures of a nematogen and an isotropic material, in the present work. It was shown that the non-nematogenic component segregates preferentially to the defect, lowering the defect free energy, and producing an increase in defect radius. As in the case of pure liquid crystals, it was observed that the effect of the second component on the radius is dramatic close to saturation conditions, where the defect radius can change by an order of magnitude with very small variations in temperature or composition. A small degree of supersaturation is possible, like in pure LCs.[19]

This study shows, with rigorous models, that the defect structure can be altered by the presence of a second component or, conversely, the solute distribution can be controlled by the defect structure. The models and theory presented can be extended to more complex defect structures, like disclination lines or three dimensional structures as in blue phases. Future work will use the present methodology to describe the role of a non-mesogenic solute on disclination interactions and disclination loop line tension.[34,35]

Appendix A: Landau–de Gennes equations in radial coordinates

In this appendix, the equations corresponding to the continuum LdG model in a radially symmetric geometry are derived. Considering that, in radial coordinates, $\nabla = \boldsymbol{\delta}_r \frac{\partial}{\partial r} + \boldsymbol{\delta}_\theta \frac{1}{r}\frac{\partial}{\partial \theta} + \boldsymbol{\delta}_\varphi \frac{1}{r\sin\theta}\frac{\partial}{\partial \varphi}$, $\frac{\partial \boldsymbol{\delta}_r \boldsymbol{\delta}_r}{\partial \theta} = \boldsymbol{\delta}_\theta \boldsymbol{\delta}_r + \boldsymbol{\delta}_r \boldsymbol{\delta}_\theta$, $\frac{\partial \boldsymbol{\delta}_r \boldsymbol{\delta}_r}{\partial \phi} = \sin\theta \boldsymbol{\delta}_\varphi \boldsymbol{\delta}_r + \sin\theta \boldsymbol{\delta}_r \boldsymbol{\delta}_\varphi$,

and for the uniaxial, radially symmetric case, $\mathbf{Q} = S(r, t)(\boldsymbol{\delta}_r \boldsymbol{\delta}_r - \mathbf{I}/3)$, where $\boldsymbol{\delta}_r$, $\boldsymbol{\delta}_\theta$, and $\boldsymbol{\delta}_\varphi$ are the unit vectors in r, θ and φ directions and $\mathbf{I}$ is the identity matrix, the gradient and divergence of $\mathbf{Q}$ are:

$$\nabla(\mathbf{Q}) = \boldsymbol{\delta}_r \boldsymbol{\delta}_r \boldsymbol{\delta}_r \frac{2\partial S}{3\partial r} + S\boldsymbol{\delta}_\theta \frac{1}{r}\frac{\partial(\boldsymbol{\delta}_r \boldsymbol{\delta}_r)}{\partial \theta} + S\boldsymbol{\delta}_\varphi \frac{1}{r\sin\theta}\frac{\partial(\boldsymbol{\delta}_r \boldsymbol{\delta}_r)}{\partial \varphi} \quad \text{(A1)}$$

$$\nabla \mathbf{Q} = \boldsymbol{\delta}_r \frac{2\partial S}{3\partial r} + \frac{2S}{r}(\boldsymbol{\delta}_r) \quad \text{(A2)}$$

Inserting in the dimensionless gradient free energy (below we drop the asterisks when referring to dimensionless variables):

$$f^g = L_{Q1}\left[4\left(\frac{S}{r}\right)^2 + \frac{4}{9}\left(\frac{\partial S}{\partial r}\right)^2\right] + L_{Q2}\left[4\left(\frac{S}{r}\right)^2 + \frac{8}{3}\frac{S}{r}\frac{\partial S}{\mathrm{d}r} + \frac{4}{9}\frac{\partial S^2}{\mathrm{d}r}\right] + L_{\phi Q2}\frac{\partial \phi}{\mathrm{d}r}\left(\frac{S}{r} + \frac{1}{3}\frac{\partial S}{\mathrm{d}r}\right) + L_\phi\left(\frac{\partial \phi}{\mathrm{d}r}\right)^2 \quad \text{(A3)}$$

The dynamic equations can be written as:

$$\frac{\partial S}{\partial t} = -\frac{\partial f^h}{\partial S} - 8\left(L_{Q1} + L_{Q2}\right)\frac{S}{r^2} - \frac{8}{3}\frac{L_{Q2}}{r}\frac{\partial S}{\mathrm{d}r} - L_{Q\phi}\frac{2}{r}\frac{\partial \phi}{\mathrm{d}r} + \frac{\partial}{\mathrm{d}r}\left[\frac{\partial f}{\partial\left(\frac{\partial S}{\partial r}\right)}\right] + \frac{2}{r}\frac{\partial f}{\partial\left(\frac{\partial S}{\partial r}\right)} \quad \text{(A4)}$$

$$\frac{\partial \phi}{\partial t} = M_\mathrm{R}\left(\frac{\partial^2}{\mathrm{d}r^2} + \frac{2}{r}\frac{\partial}{\mathrm{d}r}\right)\left(\frac{\partial f^\mathrm{h}}{\partial \phi} - \frac{\partial}{\mathrm{d}r}\left[\frac{\partial f}{\partial\left(\frac{\partial \phi}{\partial r}\right)}\right] - \frac{2}{r}\frac{\partial f}{\partial\left(\frac{\partial \phi}{\partial r}\right)}\right) \quad \text{(A5)}$$

Appendix B: derivation of analytical solutions in the macroscopic phase equilibrium approach

The purpose of this appendix is to present the full and detailed derivation of eqn (9)–(16) from eqn (7) and (8), with the adequate simplifications. First, eqn (7) and (8) are non-dimensionalized by using the characteristic length and free energy defined previously:

$$F^* = \frac{4}{3}\pi R^{*3} f_i^* + \frac{4}{3}\pi\left(D^{*3} - R^{*3}\right) f_n^* + 4\pi R^{*2}\sigma^* + \frac{16\pi S^2}{T^*}\left(D^* - R^*\right) \quad \text{(B1)}$$

$$\phi_0 D^{*3} = \phi_i R^{*3} + \phi_n (D^{*3} - R^{*3}) \quad \text{(B2)}$$

Below, we drop the asterisks when referring to dimensionless variables. As mentioned previously, the mass balance imposes a restriction so that only two variables are independent, if we consider $\phi_n = f(\phi_i, R)$, then:

$$\frac{\partial f_n}{\partial R}=\frac{\partial f_n}{\partial \phi_n}\frac{\partial \phi_n}{\partial R};\ \ \frac{\partial f_n}{\partial \phi_i}=\frac{\partial f_n}{\partial \phi_n}\frac{\partial \phi_n}{\partial \phi_i} \tag{B3}$$

In addition, it is assumed that the order parameter takes the bulk value (the distortions in the nematic phase are not strong enough to affect the degree of order) so S is a function of the composition of the nematic phase.

$$\frac{\partial S}{\partial R}=\frac{\partial S_{\mathrm{eq}}}{\partial \phi_n}\frac{\partial \phi_n}{\partial R};\ \ \frac{\partial S}{\partial \phi_i}=\frac{\partial S_{\mathrm{eq}}}{\partial \phi_n}\frac{\partial \phi_n}{\partial \phi_i} \tag{B4}$$

The surface tension is a function of the concentration jump at the interface, $\phi_I - \phi_n$.

$$\frac{\partial \sigma}{\partial R}=-\frac{\partial \sigma}{\partial \Delta\phi}\frac{\partial \phi_n}{\partial R};\ \ \frac{\partial \sigma}{\partial \phi_i}=\frac{\partial \sigma}{\partial \Delta\phi}\left(1-\frac{\partial \phi_n}{\partial \phi_i}\right) \tag{B5}$$

The derivatives of ϕ_n are obtained from eqn (A2)

$$\frac{\partial \phi_n}{\partial \phi_i}=\frac{-R^3}{(D^3-R^3)};\ \ \frac{\partial \phi_n}{\partial R}=\frac{3R^2(\phi_n-\phi_i)}{D^3-R^3} \tag{B6}$$

The equilibrium conditions are obtained by making the derivatives of the free energy with respect to the two independent variables equal to 0:

$$\frac{\partial f_i}{\partial \phi}-\frac{\partial f_n}{\partial \phi}+\frac{3}{R}\frac{\partial \sigma}{\partial \Delta\phi}\left(1+\frac{1}{(D/R)^3-1}\right)-\frac{24}{T}S\frac{\partial S_{\mathrm{eq}}}{\partial \phi}\frac{(D-R)}{(D^3-R^3)}=0 \tag{B7}$$

$$f_i-f_n+\frac{\partial f_n}{\partial \phi}(\phi_n-\phi_i)+\frac{2\sigma}{R}-\frac{3}{R}\frac{\partial \sigma}{\partial \Delta\phi}\frac{(\phi_n-\phi_i)}{(D/R)^3-1}+\frac{4S}{T}\left[6\frac{\partial S_{\mathrm{eq}}}{\partial \phi}\frac{(D-R)}{D^3-R^3}(\phi_n-\phi_i)-\frac{S}{R^2}\right]=0 \tag{B8}$$

Eqn (B7) and (B8) are the general equations describing equilibrium of a nematic and an isotropic phase in a radial configuration as given in Fig. 1. For a defect, the assumption $D \gg R$ (which leads to $\phi_n = \phi_0$) can be made, resulting in the previously shown equations:

$$\frac{\partial f_i}{\partial \phi}-\frac{\partial f_n}{\partial \phi}+\frac{3}{R}\frac{\partial \sigma}{\partial \Delta\phi}=0 \tag{B9}$$

$$(f_i-f_n)+\frac{\partial f_n}{\partial \phi}(\phi_n-\phi_i)+2\frac{\sigma}{R}-\frac{4}{T}\frac{S^2}{R^2}=0 \tag{B10}$$

Some further simplifications are made in order to obtain analytical solutions for some specific cases.

1 Close to saturation conditions

The free energy and its derivative can be linearized in the vicinity of saturation concentrations:

$$f_i \approx f_{i,\mathrm{sat}}+\frac{\partial f_{i,\mathrm{sat}}}{\partial \phi}(\phi_i-\phi_{i,\mathrm{sat}});\ \ \frac{\partial f_i}{\partial \phi}\approx\frac{\partial f_{i,\mathrm{sat}}}{\partial \phi}+\frac{\partial^2 f_{i,\mathrm{sat}}}{\partial \phi^2}(\phi_i-\phi_{i,\mathrm{sat}}) \tag{B11}$$

$$f_n \approx f_{n,\mathrm{sat}}+\frac{\partial f_{n,\mathrm{sat}}}{\partial \phi}(\phi_n-\phi_{n,\mathrm{sat}});\ \ \frac{\partial f_n}{\partial \phi}\approx\frac{\partial f_{n,\mathrm{sat}}}{\partial \phi}+\frac{\partial^2 f_{n,\mathrm{sat}}}{\partial \phi^2}(\phi_n-\phi_{n,\mathrm{sat}}) \tag{B12}$$

Introducing eqn (B11) and (B12) in eqn (B9) and (B10):

$$\frac{\partial f_{i,\mathrm{sat}}}{\partial \phi}+\frac{\partial^2 f_{i,\mathrm{sat}}}{\partial \phi^2}(\phi_i-\phi_{i,\mathrm{sat}})-\left[\frac{\partial f_{n,\mathrm{sat}}}{\partial \phi}+\frac{\partial^2 f_{n,\mathrm{sat}}}{\partial \phi^2}(\phi_n-\phi_{n,\mathrm{sat}})\right]+\frac{3}{R}\frac{\partial \sigma}{\partial \Delta\phi}=0 \tag{B13}$$

$$f_{i,\mathrm{sat}}+\frac{\partial f_{i,\mathrm{sat}}}{\partial \phi}(\phi_i-\phi_{i,\mathrm{sat}})-\left[f_{n,\mathrm{sat}}+\frac{\partial f_{n,\mathrm{sat}}}{\partial \phi}(\phi_n-\phi_{n,\mathrm{sat}})\right]+\left(\frac{\partial f_{n,\mathrm{sat}}}{\partial \phi}+\frac{\partial^2 f_{n,\mathrm{sat}}}{\partial \phi^2}(\phi_n-\phi_{n,\mathrm{sat}})\right)(\phi_n-\phi_i)+2\frac{\sigma}{R}-\frac{4}{T}\frac{S^2}{R^2}=0 \tag{B14}$$

From bulk equilibrium conditions (eqn (B7) and (B8) neglecting surface and distortion terms), the following equalities hold: $\partial f_{i,\mathrm{sat}}/\partial \phi_i = \partial f_{n,\mathrm{sat}}/\partial \phi_n$, and $f_{i,\mathrm{sat}} = f_{n,\mathrm{sat}} + \partial f_{n,\mathrm{sat}}/\partial \phi_n\,(\phi_{i,\mathrm{sat}} - \phi_{n,\mathrm{sat}})$. Introducing these relations in eqn (B13) and (B14), introducing eqn (B13) into (B14) and neglecting terms that are second order in $(\phi_n - \phi_{n,\mathrm{sat}})$

$$\phi_i-\phi_{i,\mathrm{sat}}=\frac{\partial^2 f_{n,\mathrm{sat}}/\partial \phi^2}{\partial^2 f_{I,\mathrm{sat}}/\partial \phi^2}(\phi_n-\phi_{n,\mathrm{sat}})-\frac{3}{R}\frac{\partial \sigma/\partial \Delta\phi}{\partial^2 f_{I,\mathrm{sat}}/\partial \phi^2} \tag{B15}$$

$$\frac{2\sigma-3(\partial \sigma/\partial \Delta\phi)\left(\partial^2 f_{n,\mathrm{sat}}/\partial \phi^2\right)/\left(\partial^2 f_{I,\mathrm{sat}}/\partial \phi^2\right)(\phi_n-\phi_{n,\mathrm{sat}})}{R}-\frac{4}{T}\frac{S^2}{R^2}=\frac{\partial^2 f_{n,\mathrm{sat}}}{\partial \phi^2}(\phi_{I,\mathrm{sat}}-\phi_{n,\mathrm{sat}})(\phi_n-\phi_{n,\mathrm{sat}}) \tag{B16}$$

The first equation shows that the curvature might have an effect on the concentration in the isotropic phase, given by the fact that the interfacial tension is a function of the concentration. This term is difficult to calculate or to measure experimentally. In case that the variation of the interfacial tension with composition is not significant (compared to the other terms), the equations simplify to eqn (B17) and (B18):

$$\phi_i-\phi_{i,\mathrm{sat}}=\frac{\partial^2 f_{n,\mathrm{sat}}/\partial \phi^2}{\partial^2 f_{I,\mathrm{sat}}/\partial \phi^2}(\phi_n-\phi_{n,\mathrm{sat}}) \tag{B17}$$

$$R=\frac{\sigma\pm\sqrt{\sigma^2-(4/T)\left(\partial^2 f_{n,\mathrm{sat}}/\partial \phi^2\right)(\phi_{i,\mathrm{sat}}-\phi_{n,\mathrm{sat}})(\phi_n-\phi_{n,\mathrm{sat}})S^2}}{\left(\partial^2 f_{n,\mathrm{sat}}/\partial \phi^2\right)(\phi_{i,\mathrm{sat}}-\phi_{n,\mathrm{sat}})(\phi_n-\phi_{n,\mathrm{sat}})} \tag{B18}$$

According to the simulations, the concentration in the isotropic core is very well reproduced by eqn (B17), which means that the effect of the variation of the surface energy is indeed unimportant.

2 For small concentrations

In this case, in order to find a simplified expression, some expression for the free energy of mixing has to be considered

This journal is © The Royal Society of Chemistry 2012

a priori. Using Flory–Huggins solution theory, the free energies and the derivatives for each phase can be calculated:

$$f_I - f_n = \frac{\phi_I}{v_i}\ln\phi_I - \frac{\phi_n}{r_I}\ln\phi_n + \frac{1-\phi_I}{r_{LC}}\ln(1-\phi_i)$$

$$-\frac{1-\phi_n}{r_{LC}}\ln(1-\phi_n) + \chi[\phi_i(1-\phi_i) - \phi_n(1-\phi_n)] - (1-\phi_n)f_{NEM} \tag{B19}$$

$$\frac{\partial f_n}{\partial\phi} = \frac{1}{r_I} - \frac{1}{r_{LC}} + \frac{1}{r_I}\ln\phi_n - \frac{1}{r_{LC}}\ln(1-\phi_n) + \chi(1-2\phi_n) + (1-\phi_n)\frac{\partial f_{NEM}}{\partial\phi} - f_{NEM} \tag{B20}$$

$$\frac{\partial f_i}{\partial\phi} - \frac{\partial f_n}{\partial\phi} = \frac{1}{r_I}\ln\frac{\phi_i}{\phi_n} + \frac{1}{r_{LC}}\ln\left(\frac{1-\phi_n}{1-\phi_i}\right) + \chi(2\phi_n - 2\phi_i) - (1-\phi_n)\frac{\partial f_{NEM}}{\partial\phi} + f_{NEM} \tag{B21}$$

Replacing in the equilibrium equations (eqn (B9) and (B10)), and rearranging:

$$\frac{1}{r_I}\ln\frac{\phi_i}{\phi_n} + \frac{1}{r_{LC}}\ln\left(\frac{1-\phi_n}{1-\phi_i}\right) - (1-\phi_n)\frac{\partial f_{NEM}}{\partial\phi} + \chi(2\phi_n - 2\phi_i) + f_{NEM} + \frac{3}{R}\frac{\partial\sigma}{\partial\Delta\phi} = 0 \tag{B22}$$

$$\frac{\phi_i}{r_I}\ln\frac{\phi_i}{\phi_n} + \frac{1-\phi_i}{r_{LC}}\ln\left(\frac{1-\phi_i}{1-\phi_i}\right) + \chi\phi_i[2\phi_n - \phi_i] - (1-\phi_i)f_{NEM} + \left(\frac{1}{r_I} - \frac{1}{r_{LC}} + (1-\phi_n)\frac{\partial f_{NEM}}{\partial\phi}\right)(\phi_n - \phi_i) + 2\frac{\sigma}{R} - \frac{4}{T}\frac{S^2}{R^2} = 0 \tag{B23}$$

For small concentrations, the following simplifications can be made: in the first equation the second and fourth terms will go to zero; in the second equation, the second logarithm can be linearized, and then all the terms that are second order in ϕ can be neglected. If, in addition, the variation of the surface tension with concentration is neglected as we did before, the equations reduce to:

$$\phi_I = \phi_n \exp\left[v_i\left((1-\phi_n)\frac{\partial f_{NEM}}{\partial\phi} - f_{NEM}\right)\right] \tag{B24}$$

$$R = \frac{\sigma \pm \sqrt{\sigma^2 - (4/T)[-f_{NEM} + (1 + r_I(\partial f_{NEM}/\partial\phi) - \exp[r_I((\partial f_{NEM}/\partial\phi) - f_{NEM})])(\phi_n/r_I)]S^2}}{-f_{NEM} + (1 + r_I(\partial f_{NEM}/\partial\phi) - \exp[r_I((\partial f_{NEM}/\partial\phi) - f_{NEM})])(\phi_n/r_I)} \tag{B25}$$

All the effect of the second component is comprised in the terms multiplied by ϕ_n, that add to the free energy of the nematic phase.

Acknowledgements

This work was supported in part by the U.S. Office of Basic Energy Sciences, Department of Energy, grant DE-SC0001412.

Notes and references

1 G. Goren, I. Procaccia, S. Rasenat and V. Steinberg, *Phys. Rev. Lett.*, 1989, **63**, 1237.
2 O. Mondain-Monval, J. C. Dedieu, T. Gulik-Krzywicki and P. Poulin, *Eur. Phys. J. B*, 1999, **12**, 167.
3 A. D. Rey, *Soft Matter*, 2007, **3**, 1349.
4 A. D. Rey, *Soft Matter*, 2010, **6**, 3402.
5 L. Singer, *Fuel*, 1981, **60**, 839.
6 J. Yan and A. D. Rey, *Phys. Rev. E: Stat., Nonlinear, Soft Matter Phys.*, 2002, **65**, 031713.
7 Y. Gu and N. L. Abbott, *Phys. Rev. Lett.*, 2000, **85**, 4719.
8 E. M. Terentjev, *Phys. Rev. E: Stat. Phys., Plasmas, Fluids, Relat. Interdiscip. Top.*, 1995, **51**, 1330.
9 D. Andrienko, G. Germano and M. P. Allen, *Phys. Rev. E: Stat., Nonlinear, Soft Matter Phys.*, 2001, **63**, 041701.
10 G. Gupta and A. D. Rey, *Phys. Rev. Lett.*, 2005, **95**, 127802.
11 B. Wincure and A. D. Rey, *Nano Lett.*, 2007, **7**, 1474.
12 G. E. Volovik and O. D. Lavrentovich, *Sov. Phys. JETP*, 1983, **58**, 1959.
13 O. D. Lavrentovich, *Liq. Cryst.*, 1998, **24**, 117.
14 E. C. Gartland, Jr and S. Mkaddem, *Phys. Rev. E: Stat. Phys., Plasmas, Fluids, Relat. Interdiscip. Top*, 1999, **59**, 563.
15 D. Andrienko and M. P. Allen, *Phys. Rev. E: Stat. Phys., Plasmas, Fluids, Relat. Interdiscip. Top*, 2000, **61**, 504.
16 D. de las Heras, L. Mederos and E. Velasco, *Liq. Cryst.*, 2010, **37**, 45.
17 R. Rosso and E. G. Virga, *J. Phys. A: Math. Gen.*, 1996, **29**, 4247.
18 M. Kleman and O. D. Lavrentovich, *Philos. Mag.*, 2006, **86**, 4117.
19 N. J. Mottram and T. J. Sluckin, *Liq. Cryst.*, 2000, **27**, 1301.
20 N. Schopol and T. J. Sluckin, *J. Phys.*, 1988, **49**, 1097.
21 R. Repnik, L. Mathelitsch, M. Svetec and S. Kralj, *Eur. J. Phys.*, 2003, **24**, 481.
22 P. Biscari, G. Guidoni Peroli and T. J. Sluckin, *Mol. Cryst. Liq. Cryst.*, 1997, **292**, 91.
23 P. E. Cladis, W. Van Saarloos, P. L. Finn and A. R. Kortan, *Phys. Rev. Lett.*, 1987, **58**, 222.
24 S. Zhang, E. M. Terentjev and A. M. Donald, *Liq. Cryst.*, 2005, **32**, 69.
25 S. K. Das and A. D. Rey, *Mol. Simul.*, 2005, **31**, 201.
26 S. K. Das and A. D. Rey, *Comput. Mater. Sci.*, 2006, **38**, 325.
27 A. Matsuyama, *J. Chem. Phys.*, 2008, **128**, 224907.
28 H. Yoshida, Y. Tanaka, K. Kawamoto, H. Kubo, T. Tsuda, A. Fujii, S. Kuwabata, H. Kikuchi and M. Ozaki, *Appl. Phys. Express*, 2009, **2**, 121501.
29 H. Kikuchi, M. Yokota, Y. Hisakado, H. Yang and T. Kajiyama, *Nat. Mater.*, 2002, **1**, 64.
30 J. I. Fukuda, *Phys. Rev. E: Stat., Nonlinear, Soft Matter Phys.*, 2010, **82**, 061702.
31 B. Rozic, V. Tzitzios, E. Karatairi, U. Tkalec, G. Nounesis, Z. Kutnjak, G. Cordoyiannis, R. Rosso, E. G. Virga, I. Musevic and S. Kralj, *Eur. Biophys. J.*, 2011, **34**, 17.
32 J. Lydon, *Liq. Cryst. Today*, 2006, **15**, 1.
33 E. R. Soulé and A. D. Rey, *Liq. Cryst.*, 2011, **38**, 201.
34 A. D. Rey, *Liq. Cryst.*, 1990, **37**(3), 315.
35 A. D. Rey, *Mol. Cryst. Liq. Cryst.*, 1993, **225**, 313.